The Journal of Chemical Physics

Cuprous or cupric? How substrate polarity can select for different phases of copper sulfide films in chemical bath deposition

Cite as: J. Chem. Phys. **154**, 144704 (2021); https://doi.org/10.1063/5.0046062
Submitted: 31 January 2021 • Accepted: 24 March 2021 • Published Online: 13 April 2021

Tania G. Estrada and Amy V. Walker

The Journal of Chemical Physics ARTICLE scitation.org/journal/jcp

Cuprous or cupric? How substrate polarity can select for different phases of copper sulfide films in chemical bath deposition

Cite as: J. Chem. Phys. 154, 144704 (2021); doi: 10.1063/5.0046062
Submitted: 31 January 2021 • Accepted: 24 March 2021 •
Published Online: 13 April 2021

Tania G. Estrada[1] and Amy V. Walker[1,2,a)]

AFFILIATIONS

[1] Department of Chemistry and Biochemistry, University of Texas at Dallas, Richardson, Texas 75080, USA
[2] Department of Materials Science and Engineering, University of Texas at Dallas, Richardson, Texas 75080, USA

Note: This paper is part of the JCP Special Collection in Honor of Women in Chemical Physics and Physical Chemistry.
[a)] **Author to whom correspondence should be addressed:** amy.walker@utdallas.edu

ABSTRACT

Copper sulfides have many applications from thermoelectrics to biotechnology. While the properties of different copper sulfide phases are well understood, controlling the deposited copper sulfide stoichiometry remains a significant challenge, especially in solution-phase synthesis techniques. In this work, we investigate the chemical bath deposition of Cu_xS on functionalized self-assembled monolayers (SAMs). Time-of-flight mass spectrometry, Raman spectroscopy, and x-ray photoelectron spectroscopy are employed to analyze the deposited films. We show that the use of thiourea as a sulfur source leads to the deposition of different copper sulfide phases and is controlled by the interaction of sulfur-containing ions in solution with the functionalized SAMs. For –COOH terminated SAMs, copper sulfide deposition is controlled by the surface polarity of the substrate. At the bath pH used in these experiments, the –COOH terminal groups are deprotonated. The resulting $–COO^-$ terminated SAM surface repels negatively charged sulfur-containing ions, leading to the deposition of Cu_2S. For $–CH_3$ terminated SAMs, which are non-polar, there is no specific interaction between the SAM terminal group and sulfur-containing ions and CuS is deposited. For –OH terminated SAMs, which have a polar terminal group, there are two competing effects: the repulsion of S-containing ions by the small negative charge of the terminal –OH group and the increase in the concentration of sulfur-containing ions in solution as the bath pH increases. This competition leads to the deposit stoichiometry changing from Cu_2S at pH 9 to CuS at pH 12.

I. INTRODUCTION

Copper sulfide is a low-cost, environmental-friendly semiconductor that has many applications due to its non-toxic properties[1–3] and abundance.[1,4,5] Applications of copper sulfide include in thermoelectrics,[1,5] solar cells,[6,7] energy storage,[8,9] photocatalysis,[10] biotechnology,[11–13] and nanoelectronics.[14,15] One important consideration in these applications is the controlled synthesis and deposition of the copper sulfide layer. Copper sulfide (Cu_xS_y) is known to exist in at least eight forms including the stoichiometric forms covellite (CuS) and chalcocite (Cu_2S).[1,16] Non-stoichiometric forms include spionkopite ($Cu_{1.4}S$), yarrowite ($Cu_{1.12}S$), djurleite ($Cu_{1.97}S$), geerite ($Cu_{1.6}S$), anilite (Cu_7S_4 or $Cu_{1.75}S$), and digenite (Cu_9S_5 or $Cu_{1.8}S$) phases. Each phase has a different crystal structure[1,16] and physical properties including bandgap energy, electrical resistivity, thermal conductivity, and melting points.[1] Additionally, some phases, for example, digenite and chalcocite, have allotropes.[1,16]

Copper sulfide has been synthesized by various techniques including gas phase methods such as atomic layer deposition[17] and chemical vapor deposition.[18–20] However, these methods require vacuum equipment, high temperatures, and expensive precursors. Other solution-phase routes include hydrothermal processes,[7,21–24] solvothermal deposition,[24] microwave assisted

synthesis,[25] thermolysis,[23] sonoelectrochemical deposition,[23] and chemical bath deposition (CBD).[17,26–47] Of these methods, CBD is very attractive because it is performed under ambient conditions, does not require a conductive substrate, and can be performed at low temperatures (≤50 °C), making it compatible with temperature-sensitive substrates such as organic thin films.[39]

Little is known about the role of substrate chemistry in the deposition selectivity of copper sulfides. For copper sulfide, control of deposition reactions can lead to area-selective deposition or to deposition of a specific copper sulfide phase. Previous studies have demonstrated area-selective deposition of CuS under both acidic and basic conditions. Under acidic conditions (pH ~ 2.5), CuS is preferentially deposited on $-NH_2$ terminated self-assembled monolayers (SAMs).[21,40] However, the underlying mechanism for this deposition selectivity is not understood with the effect attributed to either electrostatic interactions between CuS colloidal particles and the partially protonated $-NH_2$ terminal groups[40] or the nucleation of the CuS layer at Cu^{2+}-amine surface complexes.[26] Under basic conditions (pH 11–12) using thioacetamide, Hedlund *et al.*[41] observed that CuS preferentially deposited on $-CH_3$ terminated SAMs rather than on –OH or –COOH terminated SAMs. This behavior was attributed to a competition between the increase in chalcogenide ion concentration with an increasing bath pH and the repulsion of the chalcogenide ions with the negatively charged SAM terminal groups.

There is even less known about how the bath conditions affect the stoichiometry of the deposited copper sulfides. While a number of studies have shown that CuS deposits on substrates using thioacetamide,[41,43–45] a number of different copper sulfide phases, including CuS, $Cu_{1.97}S$, and Cu_2S, have been reported to form using thiourea.[27,28,31,33,36,38,39,42,46,47] Differences in the deposit stoichiometries have been observed to be dependent on the bath composition,[28,42] deposit film thickness,[28] and substrate.[47] However, the mechanisms underlying these effects are not well understood.

In this paper, we investigate Cu_xS CBD on $-CH_3$, –OH, and –COOH terminated SAMs under basic conditions at room temperature using thiourea as a sulfur source. Functionalized SAMs are an ideal model substrate for investigating the effects of surface chemistry on deposition processes: they are well-ordered and have a known density of terminal functional groups.[48] The two most common stoichiometric copper sulfides are CuS and Cu_2S. Chalcocite, Cu_2S, has a hexagonal close packed sulfur framework with copper atoms in triangular threefold coordination.[49] The structure of covellite, CuS, is more complicated. In the unit cell, four S atoms are part of disulfide groups, while two S atoms are isolated. The six Cu atoms also have different geometries; four have tetrahedral coordination, while the other two have trigonal coordination.[49] All the copper atoms in both structures are in the +1 oxidation state, as confirmed by x-ray photoelectron spectroscopy (XPS) measurements.[50] These similar Cu oxidation states and structural motifs make it difficult to determine the deposited copper sulfide phase using a single technique. We therefore use a multitechnique approach incorporating x-ray photoelectron spectroscopy (XPS), time-of-flight secondary ion mass spectrometry (TOF SIMS), and Raman spectroscopy in order to determine the CuS stoichiometry.

In contrast to using thioacetamide, we demonstrate that the Cu_xS phase deposited is very dependent on the interaction of the SAM terminal group with the S-containing ions in the deposition bath. On –COOH terminated SAMs, the repulsion of the chalcogenide leads to the deposition of Cu_2S. In contrast, on $-CH_3$ terminated SAMs, there is no specific interaction of the methyl terminal group with the S-containing anions and CuS is deposited. For –OH terminated SAMs, as the bath pH increases, the deposit changes from Cu_2S to CuS. In this case, as the bath pH increases, the significant increase in the concentration of S-containing ions overcomes the repulsive effect of the slightly negatively charged (δ^-) hydroxyl terminal group.

II. EXPERIMENTAL METHODS

A. Materials

All chemicals were used without further purification. Thiourea (99%) was obtained from Alfa Aesar (Thermo Fisher Scientific, Inc., Tewksbury, MA). Sodium hydroxide (≥98%, pellets) was purchased from Fisher Chemicals (Thermo Fisher Scientific, Inc., Waltham, MA). 16-mercaptohexadecanoic acid (90%) (MHA), 1-hexadecanethiol (99%) (HDT), ethylenediaminetetraacetic acid (98%) (EDTA), and copper (II) sulfate pentahydrate (98%) were purchased from Sigma-Aldrich, Inc. (St. Louis, MO). 16-Hydroxy-1-hexadecanethiol (99%) (MHL) was obtained from Frontier Scientific, Inc. (Logan, UT). Ethanol (200 proof, undenatured) was obtained from Spectrum Chemical MFG Corp (New Brunswick, NJ). Silicon ⟨111⟩ wafers were acquired from Addison Engineering, Inc., San Jose, CA.

The preparation of alkanethiolate self-assembled monolayers (SAMs) has previously been described in detail.[51–53] Briefly, gold substrates were produced by sequentially evaporating ~200 Å of chromium followed by ~1000 Å gold onto silicon wafers. A well-ordered SAM was then prepared by immersing a gold substrate into 1 mM ethanolic solution of the appropriate alkanethiol (with either a –COOH, $-CH_2OH$, or $-CH_3$ terminal group) for 24 h at room temperature. After removal from the ethanolic solution, the samples were rinsed with ethanol and dried with nitrogen gas.

B. Chemical bath deposition

The Cu_xS CBD method was adapted from the work of Hedlund *et al.*[54] The deposition bath contained 0.006M copper sulfate pentahydrate, 0.016M EDTA, and 0.012M sodium hydroxide. The pH of the deposition bath was adjusted using sodium hydroxide and sulfuric acid prior to the addition of the sulfur source, 0.012M thiourea. The SAM substrates were then quickly immersed into the deposition bath after mixing. The deposition time was 24 h except for three samples used for Raman spectroscopy where the deposition time was 48 h. After removal from the deposition bath, the samples were sonicated in water for 2 min, rinsed with deionized water, dried using nitrogen gas, and stored in a nitrogen glove box prior to further characterization.

C. X-ray photoelectron spectroscopy (XPS)

Ex situ XPS measurements were collected using a PHI VersaProbe II (Physical Electronics, Inc., Chanhassen, MN) with a

monochromatic Al Kα source (E_b = 1486.7 eV). During data collection, the chamber pressure was maintained <5 × 10^{-10} mbar. High resolution photoelectron spectra were collected with a pass energy of 23.5 eV, energy step of 0.2 eV, and analysis angle of 45°. All spectra were obtained using a charge compensation system with both electron and ion beams incident on the surface. All XPS measurements were performed within 24 h of Cu_xS CBD, and at least three samples were prepared (on different days) with multiple areas analyzed for each deposition condition. The spectra shown are representative of the data obtained.

The XPS spectra were calibrated to Au $4f_{7/2}$ binding energy (84.0 eV). Spectra were analyzed using CasaXPS 2.3.17 (RBD Instruments, Inc., Bend, OR). To determine the ratio of Cu to S, the atomic concentrations of Cu and S were obtained using Multipak 9.4.07 (Ulvac-PHI, Inc., Kanazawa, Japan).

D. Time-of-flight secondary ion mass spectrometry (TOF SIMS)

TOF SIMS data were obtained using an ION TOF IV spectrometer (ION TOF, Inc., Chestnut Hill, NY) equipped with a Bi liquid metal ion gun. The instrument has three vacuum chambers for sample introduction, preparation, and analysis. The preparation and analysis chambers were maintained at <5 × 10^{-9} mbar during data collection. The primary Bi^+ ions had a kinetic energy of 25 keV and were contained in a ~100 nm diameter probe beam, which was rastered over a (100 × 100) μm^2 area. All spectra were acquired with a total ion dose of less than 10^{11} ions cm^{-2}, which is within the static SIMS regime.[55] The secondary ions were extracted into a time-of-flight mass spectrometer using a potential of 2000 V and were reaccelerated to 10 keV before reaching the detector. At least three areas on each sample were analyzed, and the spectra shown are representative of the data.

E. Raman spectroscopy

Raman spectra were collected using a Thermo Scientific DXR Raman microscope (Thermo Scientific, Madison, WI) equipped with a 532 nm diode laser, 50× objective lens and 25 μm slit aperture. The spectra were collected using a laser power of 0.1 mW with an estimated spot diameter of 0.7 μm. In order to reduce interference from fluorescence, "fluorescence correction" was used and the samples photobleached to data collection.

III. RESULTS AND DISCUSSION

The XPS data clearly show that multiple types of copper sulfide are deposited and that the chemical identity of the Cu_xS deposit is dependent on both the bath pH and the SAM terminal group. Figure 1 displays the ratio of the Cu to S atomic concentrations, Cu/S, with deposition bath pH. For $-CH_3$ terminated SAMs, Cu/S is equal to 1.0 within experimental error for all deposition bath pH studied, indicating that CuS is deposited. In contrast, for –COOH terminated SAMs, Cu/S is 2.0 within experimental error for all deposition bath pH, which is consistent with the deposition of Cu_2S. In Fig. 1, it can also be clearly seen that for –OH terminated SAMs, Cu/S decreases from 2.0 to 1.0 (within experimental error) as the deposition bath pH increases from pH 9 to pH 12.

The x-ray photoelectron and Auger electron data agree with the measured Cu/S ratios. Figure 2 displays the variation of the Cu 2p and S 2p x-ray photoelectron spectra of the deposited Cu_xS films on

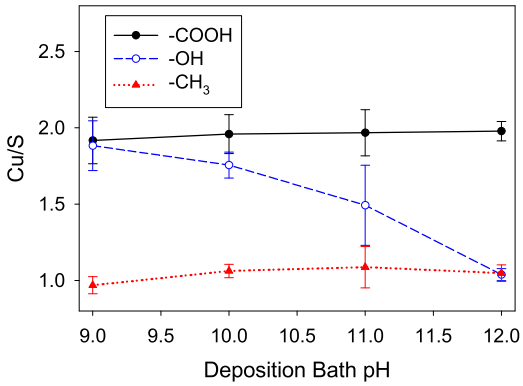

FIG. 1. Variation of the ratio of Cu to S (Cu/S) after Cu_xS CBD with bath pH on $-CH_3$, –OH, and –COOH terminated SAMs. Deposition conditions: 24 h, room temperature.

$-CH_3$, –OH, and –COOH terminated SAMs after 24 h with deposition bath pH. Table I also summarizes the x-ray photoelectron and Auger electron data. For every deposition bath pH and functionalized SAM, the Cu $2p_{3/2}$ binding energies are 931.6 ± 0.2 eV and the difference between the Cu $2p_{3/2}$ and Cu $2p_{1/2}$ binding energies is 19.8 ± 0.2 eV, which is consistent with the deposition of CuS.[33,50,56–61] However, the S 2p binding energy and photoelectron spectra indicate that there are multiple copper sulfides deposited. Although S 2p cannot be resolved into $2p_{3/2}$ and $2p_{1/2}$ peaks, on $-CH_3$ terminated SAMs, the S 2p binding energies, 162.1 ± 0.1 eV, are consistent with the deposition of CuS.[56,61,62] Furthermore, on –COOH terminated SAMs, the S 2p binding energy, 161.8 ± 0.1 eV, indicates that Cu_2S is deposited[56,61] (Table I). Additionally, on $-CH_3$ terminated SAMs, the S 2p photoelectron peak has a full width half maximum (FWHM) of ~2.8 eV and it is larger than on –COOH terminated SAMs, ~2.2 eV. These observations suggest that on $-CH_3$ terminated SAMs, the S 2p photoelectron peak is composed of two doublets of the S^{2-} and S_2^- ligands present in CuS.[56] On –OH terminated SAMs, the S 2p binding energy increases from 161.8 to 162.2 eV as the deposition bath pH increases (Table I). Furthermore, the FWHM of the S 2p peak increases from ~2.2 to ~2.9 eV. Taken together, these data indicate that on –OH terminated SAMs at pH 9 the deposit is composed of Cu_2S, and as the deposition bath pH increases, the deposit changes to CuS. The Cu LMM kinetic energies and peak shapes[57,59,60] (Fig. 3, Table I) are also consistent with the deposition of CuS and Cu_2S on $-CH_3$ and –COOH terminated SAMs. Furthermore, the Cu LMM data indicate that on –OH terminated SAMs, the deposit changes from Cu_2S to CuS as the deposition bath pH increases [Fig. 3(b)]. After deposition at pH 9, the Cu LMM peak shapes and kinetic energy are similar to those observed for the Cu_2S film formed on –COOH terminated SAMs. As the bath pH increases, the Cu LMM peak shape and kinetic energy evolve until at pH 12 the peak has a similar shape and energy for the CuS film deposited on $-CH_3$ terminated SAMs. Kundu *et al.*[59] also observed comparable changes in X-ray Auger Electron Spectra (XAES) during the sulfurization of Cu substrates to copper sulfide.

Finally, the modified Auger parameter (α'), which is the sum of the Cu $2p_{3/2}$ binding energy and Cu LMM kinetic energy, also

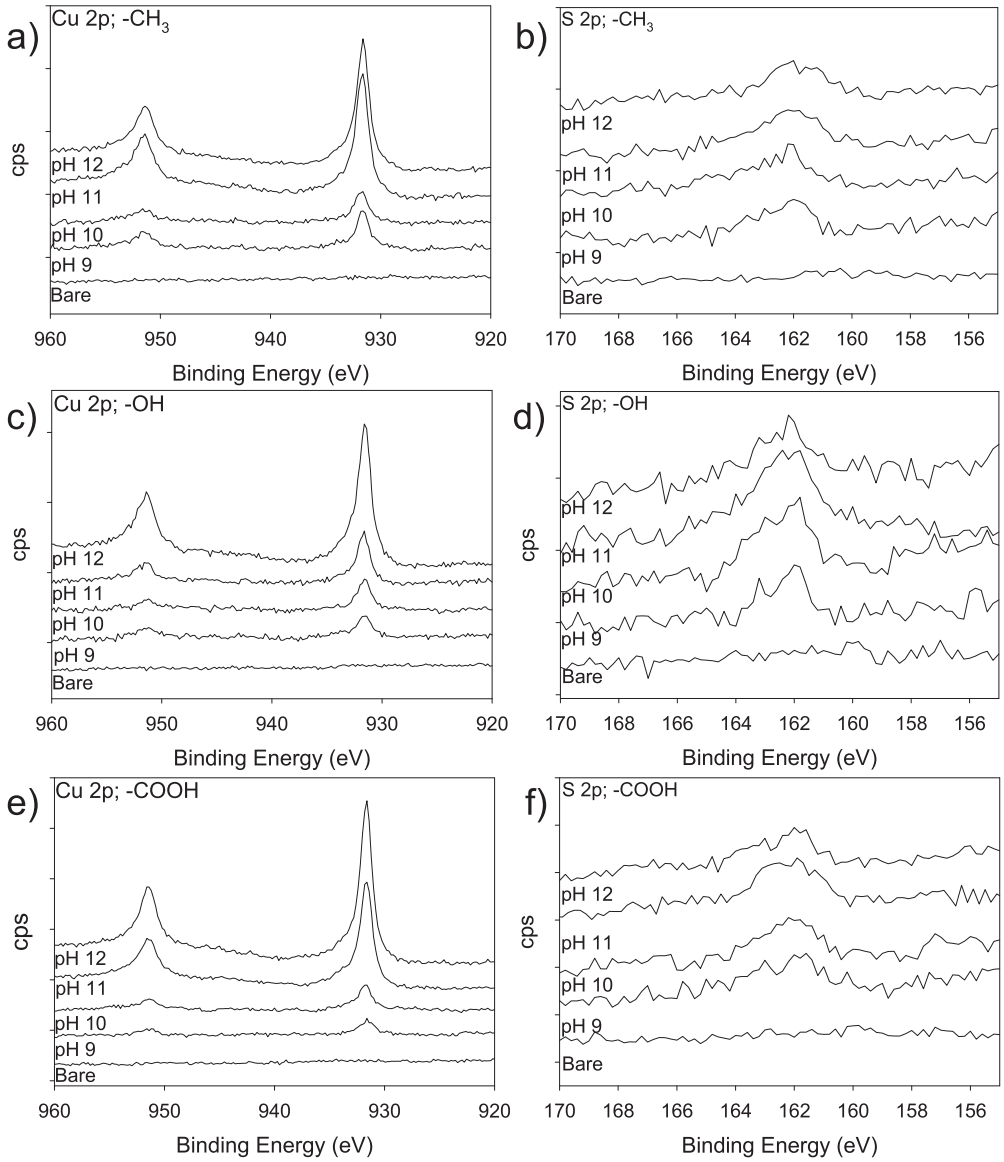

FIG. 2. Variation of Cu 2p and S 2p photoelectron spectra after Cu_xS CBD on [(a) and (b)] $–CH_3$, [(c) and (d)] –OH, and [(e) and (f)] –COOH terminated SAMs with bath pH at room temperature. Deposition time: 24 h. Also shown for reference are the spectra for the bare SAMs.

indicates that the stoichiometry of the deposited Cu_xS layer is dependent on both the SAM functional group and bath pH (Table I). Consistent with the deposition of CuS[56,57,61] on $–CH_3$ terminated SAMs for all deposition bath pH, α' is 1850.1 ± 0.2 eV (Table I). Similarly, on –COOH terminated SAMs for all deposition bath pH, the modified Auger parameters are 1849.8 ± 0.2 eV (Table I), which are consistent with the deposition of Cu_2S.[56,57,61] Finally, in Table I, it can be clearly seen that on –OH terminated SAMs, the deposition bath pH α' increases from 1849.8 to 1850.1 eV, confirming that the deposit chemistry changes from Cu_2S to CuS.

We note that both the C 1s and O 1s photoelectron spectra show that there is no, or little, interaction between the deposited SAMs and the copper sulfide layer; there are no new photoelectron peaks observed in the spectra (see the supplementary material). Briefly, the data show that as the deposition bath pH increases, the binding energies of the C 1s and O 1s photoelectron peaks increase and then decrease. Similarly, the intensities of these peaks increase and decrease as the deposition bath pH increases. These changes are likely due to charge transfer between the copper sulfide deposits and the gold substrate mediated by the dipole moment of the functionalized SAMs. We note that similar effects have been observed for MoS_2 deposited on functionalized SAMs[63] and Au clusters deposited on rutile.[64]

Finally, the XPS data also suggest that the amount of Cu_xS deposited is dependent on the bath pH but not on the chemical identity of the SAM functional group in contrast to CuS CBD using

TABLE I. Cu $2p_{3/2}$ and S 2p binding energies, Cu LMM kinetic energies, and modified Auger parameter, α', after Cu_xS CBD for 24 h on –COOH, –OH, and $–CH_3$ terminated SAMs at room temperature.

SAM terminal group	Deposition bath pH	Binding energy Cu $2p_{3/2}$ (eV)	Kinetic energy Cu LMM (eV)	Binding energy S 2p (eV)	α' (eV)
–COOH	9	931.6	918.2	161.8	1849.8
	10	931.5	918.4	161.8	1849.9
	11	931.6	918.2	161.9	1849.8
	12	931.6	918.2	161.8	1849.8
–OH	9	931.6	918.2	161.8	1849.8
	10	932.0	917.8	162.0	1849.8
	11	931.7	918.4	162.0	1850.1
	12	931.6	918.5	162.2	1850.1
$–CH_3$	9	931.6	918.5	162.1	1850.1
	10	931.6	918.5	162.0	1850.1
	11	931.6	918.4	162.1	1850.0
	12	931.6	918.4	162.2	1850.0

thioacetamide.[41] Figure 4 displays the Cu $2p_{3/2}$ photoelectron peak height with bath pH after Cu_xS deposition for 24 h on $–CH_3$, –OH, and –COOH terminated SAMs. The Cu $2p_{3/2}$ peak height can be used as a quantitative measure of the amount of Cu_xS deposited because it is related to the peak area. Furthermore, there are no overlapping peaks in the photoelectron spectra that can lead to inaccuracies in the quantitative estimation. We also note that our previous studies of CuS CBD on functionalized SAMs using thioacetamide show that Cu $2p_{3/2}$ peak heights are consistent with film thicknesses measured using the AFM.[41] In Fig. 4, it can be clearly seen that the Cu $2p_{3/2}$ peak height increases with increasing bath pH, indicating that more Cu_xS has been deposited. Furthermore, at each deposition bath pH, the Cu $2p_{3/2}$ peak heights are the same (within experimental error), indicating that the same amount of Cu is present on each functionalized SAM. Since Cu_2S is deposited on –COOH terminated SAMs, these data suggest that the deposited layer is thinner than on $–CH_3$ terminated SAMs where CuS is deposited.

The Raman spectroscopic and TOF SIMS measurements agree with the XPS data. Figure 5 displays Raman spectra after Cu_xS deposition on $–CH_3$, –OH, and –COOH terminated SAMs at room temperature for 48 h. We note that similar results are obtained after Cu_xS deposition for 24 h, but the spectra have a lower signal-to-noise ratio. In Fig. 5(a), it can be clearly seen that after deposition at pH 12, there are several spectral features observed. On $–CH_3$ and –OH terminated SAMs, there is a peak at ~471 cm^{-1}, while on –COOH terminated SAMs, a peak is observed at ~468 cm^{-1}, which are assigned as the ν(S–S) stretching modes of CuS and Cu_2S, respectively.[31,65–68] Additionally, after CuS deposition on –OH and $–CH_3$ terminated SAMs, there is a broad peak centered at ~280 cm^{-1}, which is assigned as a lattice mode (A_{1g} TO).[31] On –COOH terminated SAMs, there is also a weak broad peak centered at a higher frequency, ~295 cm^{-1}, which we also assign as a lattice mode. Figure 5(b) displays Raman spectra after Cu_xS deposition on –OH terminated SAMs with varying pH. As the deposition bath pH increases, the frequency of the ν(S–S) stretching mode increases from 468 to 471 cm^{-1}, indicating that the deposit has changed from Cu_2S at pH 10 to CuS at pH 12.

For all experimental conditions and functionalized SAMs studied, the TOF SIMS spectra indicate that Cu_xS is deposited. As the deposition bath pH increases, the ions characteristic of the functionalized SAMS, such as Au_2M^- [where M = $–S(CH_2)_{15}COOH$, $–S(CH_2)_{15}CH_2OH$, or $–S(CH_2)_{15}CH_3$], decrease, indicating that the substrate is increasingly covered by the Cu_xS layer. This suggests that more CuS is deposited as the deposition bath pH increases. Furthermore, information about the chemistry of the deposited Cu_xS layers can be obtained by examination of the $Cu_xS_y^{\pm}$ ions formed. Copper (I) sulfide has a hexagonal close packed sulfur framework with the copper atoms mainly in trigonal coordination, and hence, it is expected that characteristic $CuS_3^{\pm}$ ions are present in the SIMS spectra.[16,49] For copper (II) sulfide, the copper atoms have trigonal and tetrahedral coordination and the sulfur atoms have trigonal bipyramidal and tetrahedral (with a disulfide unit) coordination.[49] It is therefore expected that the characteristic ions of CuS are $CuS_3^{\pm}$, $CuS_4^{\pm}$, $Cu_5S^{\pm}$, $Cu_3S_2^{\pm}$, and S_2^-. On –COOH terminated SAMs, $Cu_2S^{\pm}$, S_2^-, and $CuS_3^{\pm}$ ions are observed after Cu_2S deposition for 24 h at pH 12. In contrast, on $–CH_3$ terminated SAMs, $Cu_2S^{\pm}$, S_2^-, $Cu_3S_2^-$, CuS_4^-, and $CuS_3^{\pm}$ ions are observed after CuS deposition for 24 h at pH 12. Interestingly, the data show that the $Cu_2S^{\pm}$ and $CuS_3^{\pm}$ ions have different intensities (peak areas) between CuS deposited on $–CH_3$ terminated SAMs and Cu_2S formed on –COOH terminated SAMs (Fig. 6). In Fig. 6(a), in the negative ion spectra, on –COOH terminated SAMs, the Cu_2S^- and CuS_3^- ion intensities are much larger than $(CH)_{10}SH^-$, a characteristic ion of the bare SAMs. In contrast, on $–CH_3$ terminated SAMs, the Cu_2S^- and CuS_3^- ion intensities are approximately the same, or lower, than the $(CH)_{10}SH^-$ ion intensity [Fig. 6(c)]. In contrast, in the positive ion spectra, after deposition on $–CH_3$ terminated SAMs, the ion intensities of CuS_3^+ are ~9× larger than the ion intensity of Cu_2S^+ [Fig. 6(d)]. On –COOH terminated SAMs, the ion intensities of Cu_3S^+ are only ~3× larger than the ion intensities of Cu_2S^+ [Fig. 6(b)]. These observations indicate that TOF SIMS spectra can be employed to differentiate between Cu_2S and CuS. Furthermore, the Cu_2S^+ and CuS_3^+ ion intensities are generally lower on –COOH

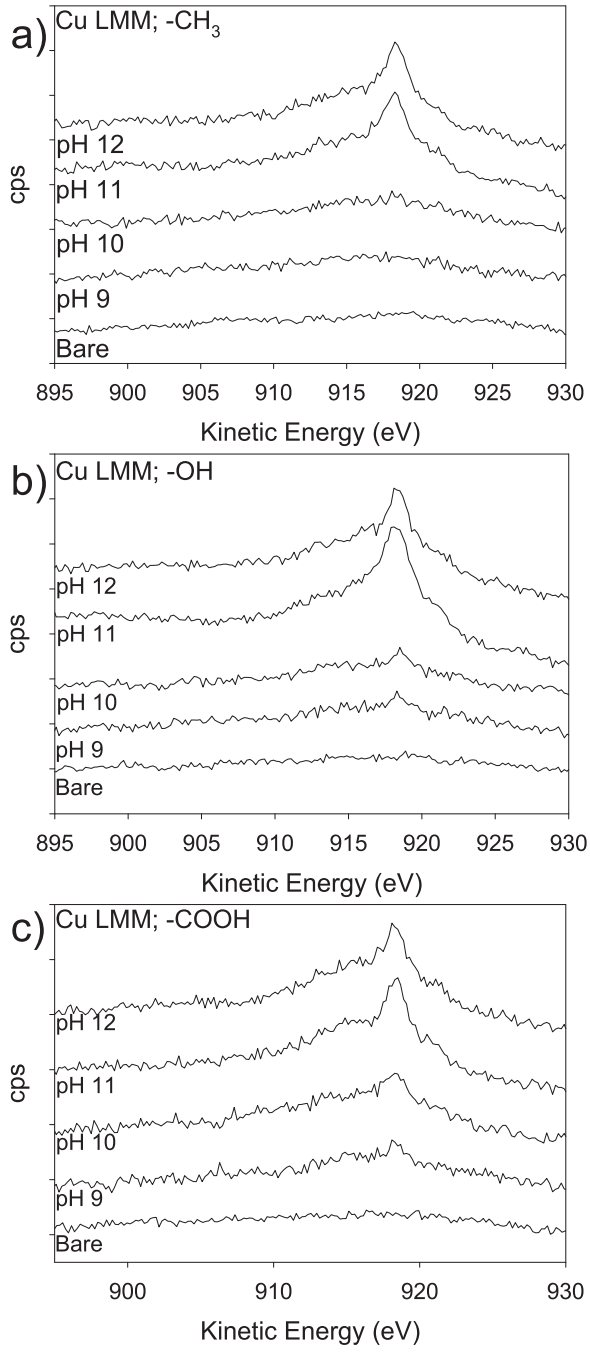

FIG. 3. Variation of XAES Cu LMM transitions of the Cu_xS films deposited on (a) $–CH_3$, (b) –OH, and (c) –COOH at room temperature. Deposition time: 24 h. Also shown for reference are the spectra for the bare SAMs.

terminated SAMs than on $–CH_3$ terminated SAMs. In Fig. 7, high resolution negative ion spectra are shown centered at m/z 160.5 after Cu_xS CBD on –OH terminated SAMs. After deposition at pH 9, the ion intensities of Cu_2S^- and Cu_3S^- are similar to those

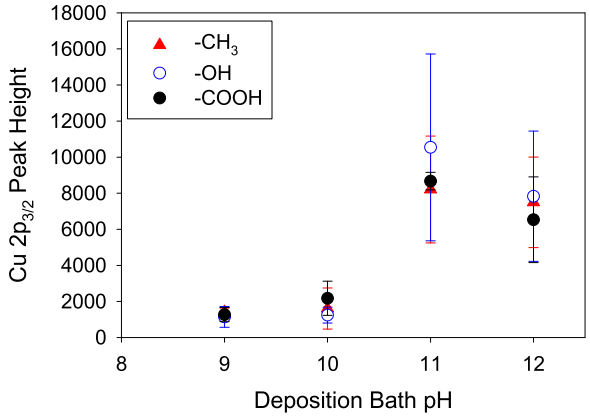

FIG. 4. Variation of the Cu $2p_{3/2}$ peak height after Cu_xS CBD on $–CH_3$, –OH, and –COOH terminated SAMs for 24 h at room temperature.

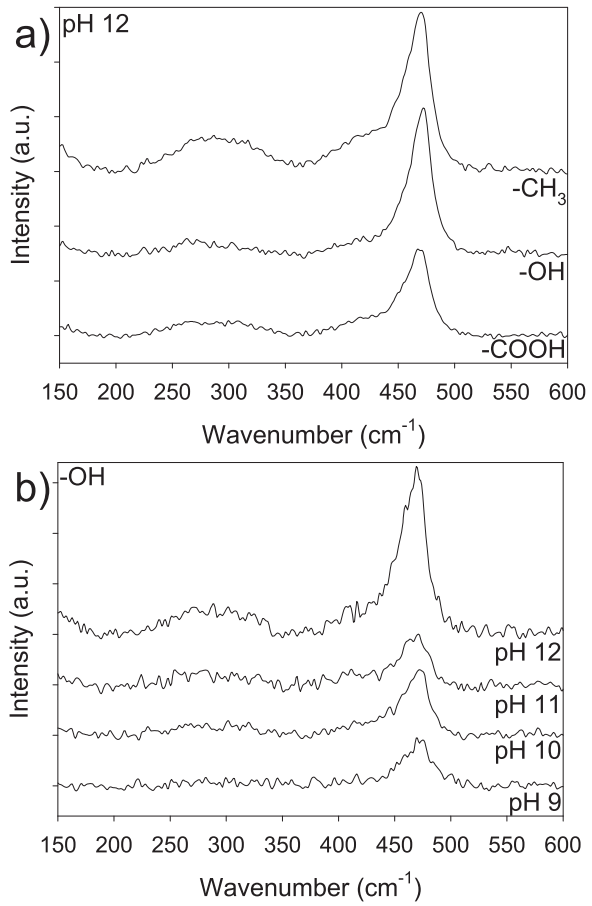

FIG. 5. Raman spectra after Cu_xS CBD for 48 h at room temperature (a) on $–CH_3$, –OH, and –COOH terminated SAMs at pH 12 and (b) on –OH terminated SAMs as the bath pH is varied between pH 9 and pH 12.

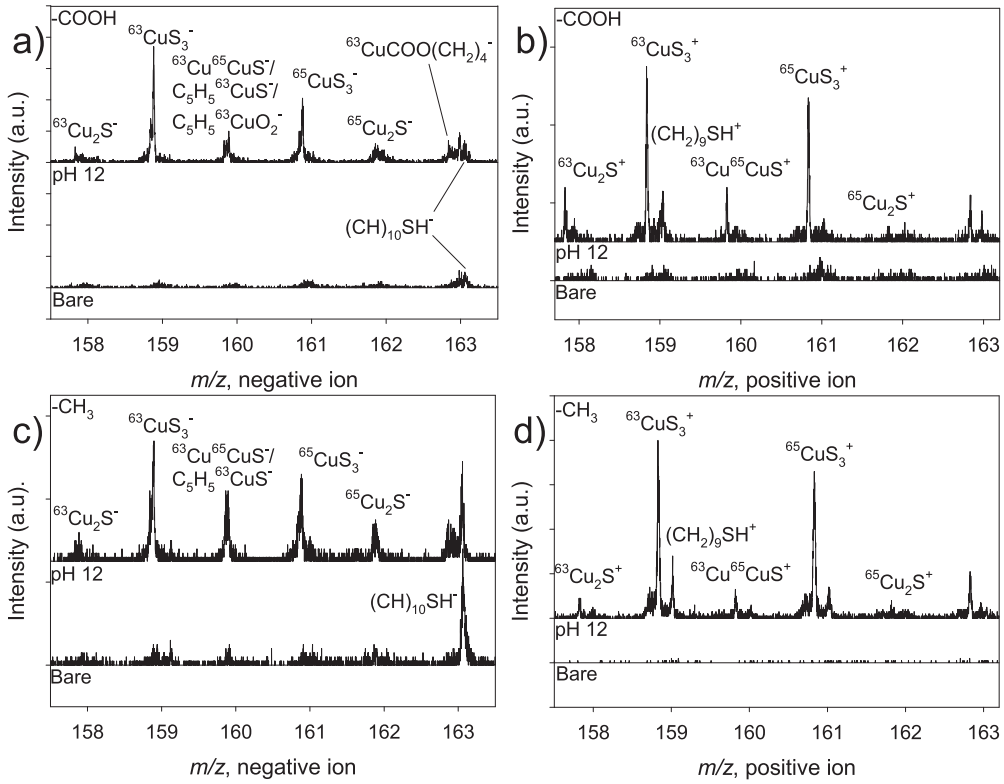

FIG. 6. High resolution [(a) and (c)] negative and [(b) and (d)] positive ion mass spectra centered at *m/z* 160.5 after Cu_xS CBD for 24 h at pH 12 and room temperature on [(a) and (b)] –COOH and [(c) and (d)] –CH_3 terminated SAMs. Also shown for reference are the mass spectra of the functionalized SAMs before deposition ("bare").

observed for $(CH)_{10}SH^-$, indicating that Cu_2S is deposited. In contrast, after deposition at pH 12, the ion intensities of Cu_2S^- and Cu_3S^- are lower than those of $(CH)_{10}SH^-$, indicating that CuS is deposited. Taken together, the data confirm that on –OH terminated SAMs, the copper sulfide stoichiometry is dependent on the deposition bath pH. Finally, for –COOH terminated SAMs, we observe ions of the form $CuCOO(CH_2)_x(CH)_y{}^+$ and $CuCOO(CH_2)_x{}^-$ indicating that the Cu^{2+} ions interact with the –COOH terminal group [Fig. 6(a)] and are characteristic of copper–carboxylate complexes.

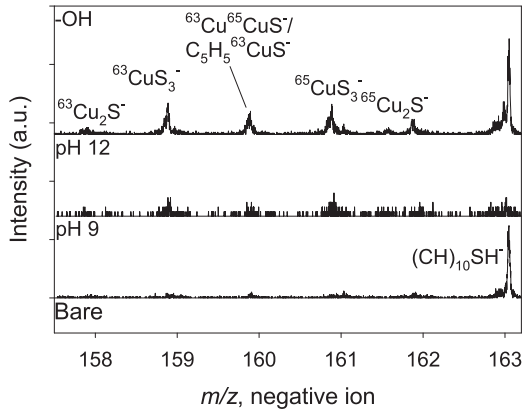

FIG. 7. Variation of high resolution negative ion mass spectra centered at *m/z* 160.5 after Cu_xS CBD for 24 h at pH 9 and pH 12 on –OH terminated SAMs. Deposition temperature: room temperature. Also shown for reference are the mass spectra of the –OH terminated SAM before deposition ("bare").

A. Reaction pathways

Copper sulfides were one of the first materials to be deposited using CBD. While there have been many studies of Cu_xS, there is no consensus about the reaction pathways involved. In CBD reactions, a controlled reaction is employed to deposit a thin film on a substrate via a precipitation reaction. In this case, Cu_xS is deposited via the decomposition of thiourea in an alkaline solution containing a copper salt. The reaction can be described using the following (unbalanced) chemical reaction (reaction pathway):[39,41,54]

$$Cu^{2+} + EDTA^{4-} \rightarrow [Cu(EDTA)]^{2-}, \quad (1)$$

$$SC(NH_2)_2 + OH^- \rightarrow CN_2H_2 + H_2O + HS^-, \quad (2)$$

$$HS^- + OH^- \rightarrow S^{2-} + H_2O, \quad (3)$$

$$Cu^{2+} + S^{2-} \rightarrow CuS. \quad (4)$$

In reaction (1), the concentration of "free" copper ions is controlled using the complexing agent ethylenediaminetetraacetic acid (EDTA). The formation of bisulfide ions, HS^-, occurs via the reaction of thiourea with hydroxide ions [reaction (2)].[39,69]

Subsequently, the bisulfide ions decompose to form S^{2-} ions [reaction (3)],[39] which then react with copper ions to form CuS [reaction (4)]. By Le Chatelier's principle, as the bath pH increases (concentration of OH^- increases), reactions (2) and (3) are driven to the product side, leading to the production of more S^{2-}. This leads to a higher production of CuS [reaction (4)], as experimentally observed (Fig. 4).

While reactions (2) and (3) clearly show that as the bath pH increases, the rate deposition increases, the above reaction pathway does not account for the following observations:

(a) Cu_2S and CuS is deposited in contrast to CuS CBD using thioacetamide where CuS is deposited on these functionalized SAMs;
(b) on –COOH terminated SAMs, Cu_2S is deposited for all bath pHs;
(c) on $–CH_3$ terminated SAMs, CuS is deposited for all bath pHs; and
(d) on –OH terminated SAMs, Cu_2S is deposited at pH 9 and the ratio of Cu to S decreases until at pH 12 CuS is deposited.

We propose that in Cu_xS CBD, thiourea plays multiple roles in the deposition by acting as a reducing agent, a complexing agent, and a sulfur source. Upon mixing Cu^{2+} ions and thiourea in excess concentration, it is well known that copper (II) ions are rapidly reduced to Cu^+ via the following reaction:[70–73]

$$2Cu^{2+} + 2SC(NH_2)_2 \rightarrow (-SC(NH)NH_2)_2^{2+} + 2Cu^+. \quad (5)$$

The reaction product, Cu^+, then reacts with thiourea to form copper–thiourea complexes,[70,71,73]

$$Cu^+ + nSC(NH_2)_2 \rightarrow \left[Cu\left(SC(NH_2)_2\right)_n\right]^+. \quad (6)$$

The concentration of Cu^+ is, therefore, dependent on the concentration of "free" Cu^{2+} [reaction (1)], the relative rates of thiourea hydrolysis [Eq. (2)], and the redox/complexation reaction [reactions (5) and (6)]. Furthermore, the formation of Cu^+ is consistent with the formation of CuS and Cu_2S, which can be considered to be Cu(I) compounds with the formulas $(Cu^+)_3(S^{2-})(S_2^-)$ and $(Cu^+)_2(S^{2-})$, respectively.[50,74]

Thiourea also hydrolyzes to form the bisulfide ion, HS^-, reaction (2), leading to the formation of sulfide ions, S^{2-} [reaction (3)]. The sulfide ion can react with copper (I) ions to form cuprous sulfide,

$$2Cu^+ + S^{2-} \rightarrow Cu_2S. \quad (7)$$

Once formed, the sulfide ions can further react to form S_2^{2-}, which is one of the dominant polysulfides at these bath pHs,[75,76] by, for example,[77]

$$2S^{2-} + 2H_2O \rightarrow S_2^{2-} + 2OH^- + H_2. \quad (8)$$

It is also possible that HS^- reacts with dissolved oxygen [reaction (9)] or sulfate ions present (from the copper source) [reaction (10)] to form S_2^{2-} by reactions such as[75,76,78]

$$2HS^- + \frac{1}{2}O_2 \rightarrow S_2^{2-} + H_2O, \quad (9)$$

$$SO_4^{2-} + H^+ + 7HS^- \rightarrow 4S_2^{2-} + 4H_2O. \quad (10)$$

Once formed, the disulfide and sulfide ions can react with Cu^+ ions to form CuS,

$$3Cu^+ + S^{2-} + S_2^{2-} \rightarrow \left(Cu^+\right)_3\left(S^{2-}\right)\left(S_2^-\right) + e^-. \quad (11)$$

In reaction (11), the disulfide ion is oxidized and the excess electron is adsorbed by a side reaction, such as the decomposition of S_2^{2-} to form S^{2-} ions. We note that the reaction of S_2^- with Cu^+ is very unlikely to occur because the formation of copper disulfide, CuS_2, only occurs at very high pressures and temperatures.[79] The presence of Cu^+, Cu^{2+}, S_2^{2-}, and S^{2-} ions in solution [reactions (1), (3), (5), and (8)–(10)] is also consistent with formation of non-stoichiometric copper sulfides, as observed for Cu_xS deposition on –OH terminated SAMs (Fig. 3). For example, at pH 10, $Cu_{1.75}S$ is deposited, which can be formed via the following reaction:

$$6Cu^+ + Cu^{2+} + 4S^{2-} \rightarrow \left(Cu^+\right)_6\left(Cu^{2+}\right)\left(S^{2-}\right)_4. \quad (12)$$

The above reaction pathways show that Cu_xS $1 \le x \le 2$ can be deposited in CBD but do not explain the reaction selectivity. Furthermore, they do not explain why CuS is deposited using thioacetamide as a sulfur source while the copper sulfide deposit chemistry varies using thiourea. The deposition of copper sulfide, CuS, reaction (11), requires the formation of Cu(I) and disulfide ions. Similar to thiourea, thioacetamide has been shown to reduce Cu(II) to Cu(I) when thioacetamide is present in excess concentration, leading to the formation of copper-thioacetamide species.[80–82] These copper–thioacetamide species rapidly decompose in solution, leading to the formation of copper sulfide.[80] Under basic conditions, the hydrolysis of thioacetamide to form the bisulfide ion is more rapid by at least an order of magnitude than for thiourea, and hence, the concentrations of the sulfides, bisulfides, and disulfides in solution are much higher.[69,83] Thus, copper sulfide, CuS, is deposited under basic conditions on these functionalized SAMs, as experimentally observed.[41]

If the reaction was solely dependent on the solubility product of copper sulfides, then Cu_2S would deposit on all functionalized SAMs; the solubility product, K_{sp}, of Cu_2S, 2.5×10^{-48}, is more than 10 orders of magnitude lower than the K_{sp} of CuS (6.3×10^{-36}).[84] Our data clearly show that this is not the case (Fig. 1). We propose that Cu_xS deposition on functionalized SAMs occurs via a kinetically controlled mechanism in which S-containing anions modulate the deposition reaction.

Both –OH and –COOH terminated SAMs have polar terminal groups. Furthermore, the carboxylic acid group can deprotonate to form carboxylate ions, $–COO^-$. The surface $pK_{1/2}$ of –COOH terminated SAMs is ~8.0,[85] which is the solution pH at which the terminal groups are 50% ionized. As the bath pH increases from pH 9 to pH 12, the carboxylic acid terminated SAM surface becomes increasingly deprotonated; at pH 9, ~90.9% of the terminal groups are $–COO^-$, while at pH 12, ~99.99% of the surface is covered by $–COO^-$. The surface can therefore form Cu^{2+}–carboxylate (or less likely Cu^+–carboxylate) complexes, which can act as nucleation sites for CuS deposition. However, the complexing constant of Cu^{2+} with carboxylic acids (<100)[86] is very low compared to the binding constant of Cu^{2+} with EDTA (5×10^{18})[84] and the fast redox reaction between Cu^{2+} and thiourea.[70] Thus, copper sulfide deposition on –COOH terminated SAMs is dominated by the surface polarity of the substrate. At the deposition bath pH employed in these experiments, the

deprotonated $-COO^-$ terminal groups repel the negatively charged S-containing anions in solution. Since HS^- and S^{2-} are the dominant sulfur species in the solution, the deposition proceeds via reaction (7) and Cu_2S is deposited at all bath pHs.

Hydroxyl-terminated SAMs have a polar terminal C–OH bond but do not deprotonate under the experimental conditions employed. In this case, the dipole of the terminal CH_2–OH group is such that the –OH group has a small negative charge, δ^-. At pH 9, the concentration of the negatively charged S species [reactions (2), (3), and (8)–(10)] is lower than at pH 12, and hence, at pH 9, the deposition is dominated by the repulsion of the S-containing anions with the negatively charged –OH terminated surface. Thus, at pH 9, copper(I) ions react with the dominant S species in solution, S^{2-}, leading to the deposition of Cu_2S in a similar manner to that observed on –COOH terminated SAMs. As the bath pH increases, the concentration of sulfur species, such as S^{2-}, HS^-, and S_2^-, significantly increases [reactions (2), (3), and (8)–(10)], and so the effect of the surface repulsion effectively decreases. Thus, as the deposition bath pH increases, the Cu_xS deposit stoichiometry slowly changes from Cu_2S at pH 9 to CuS at pH 12 (Fig. 3 and Table I).

In contrast, for $-CH_3$ terminated SAMs, the C–H bonds of the methyl terminal group are non-polar. There is, therefore, no specific reaction between copper and sulfur ions in solution and the SAM terminal group, and thus, the effective concentration of S^{2-}, S_2^{2-}, and other S-containing anions is higher at the solution/$-CH_3$ terminated SAMs for all bath pHs employed. This suggests that CuS will deposit on the substrate via reaction (11), as experimentally observed.

IV. CONCLUSIONS

The chemical bath deposition of copper sulfide is strongly dependent on the interaction of the S-containing anions with the SAM functional groups. Using thiourea as the S source leads to the deposition of different copper sulfide phases.

For –COOH terminated SAMs, the deposition is controlled by the surface polarity of the substrate. At the deposition bath pH employed, the carboxylic acid terminal groups are deprotonated, leading to the formation of a $-COO^-$ terminated SAM surface. The negatively charged carboxylate terminal groups repel the S-containing anions in solution. Since HS^- and S^{2-} are the dominant sulfur species in the solution, Cu_2S is deposited at all bath pHs. In contrast, for $-CH_3$ terminated SAMs, there is, therefore, no specific reaction between copper and sulfur ions in solution and CuS is deposited.

For –OH terminated SAMs, there are two competing effects: the repulsion of S-containing ions by the small negative charge of the terminal –OH group and the increase in S-containing anions in solution as the bath pH increases. As the bath pH increases, the Cu_xS deposit stoichiometry changes from Cu_2S at pH 9 to CuS at pH 12. At pH 9, the deposition is dominated by the repulsion of S-containing anions with the negatively charged –OH terminated surface and Cu_2S is deposited. As the bath pH increases, the concentration of sulfur species, such as S^{2-}, HS^-, and S_2^-, significantly increases and the effect of the terminal group-solution repulsion decreases, leading to deposits with lower Cu/S ratios.

These experiments indicate that CBD can not only be employed for area-selective deposition but also for controlling the deposit stoichiometry, broadening the applications of films deposited by CBD.

SUPPLEMENTARY MATERIAL

See the supplementary material for high resolution C 1s and O 1s photoelectrons of Cu_xS films deposited on $-CH_3$, –OH, and –COOH terminated SAMs for 24 h, room temperature, and bath pH.

DEDICATION

This paper honors Ruth Lynden-Bell who is not only a leader in molecular simulations but has also inspired many students, including one of the authors (A.V.W.), to pursue careers in chemical physics/physical chemistry.

ACKNOWLEDGMENTS

The authors gratefully acknowledge support from the National Science Foundation (Grant No. CHE 1708259) and thank Jenny K. Hedlund who performed preliminary experiments on CuS CBD using thiourea.

DATA AVAILABILITY

The data that support the findings of this study are available from the corresponding author upon reasonable request.

REFERENCES

[1] R. Mulla and M. H. K. Rabinal, Energy Technol. **7**, 1800850 (2019).
[2] A. Shah, P. Torres, R. Tscharner, N. Wyrsch, and H. Keppner, Science **285**, 692–698 (1999).
[3] A. Polman, M. Knight, E. C. Garnett, B. Ehrler, and W. C. Sinke, Science **352**, aad4424 (2016).
[4] G. B. Haxel, S. Boore, and S. Mayfield, in *U.S. Geological Survey Fact Sheet 087-02*, edited by P. H. Stauffer and J. W. Hendley II (2002), https://pubs.usgs.gov/fs/2002/fs087-02.
[5] A. V. Powell, J. Appl. Phys. **126**, 100901 (2019).
[6] H. Lee, S. W. Yoon, E. J. Kim, and J. Park, Nano Lett. **7**, 778–784 (2007).
[7] Y. Wu, C. Wadia, W. Ma, B. Sadtler, and A. P. Alivisatos, Nano Lett. **8**, 2551–2555 (2008).
[8] Y. Wang, F. Liu, Y. Ji, M. Yang, W. Liu, W. Wang, Q. Sun, Z. Zhang, X. Zhao, and X. Liu, Dalton Trans. **44**, 10431–10437 (2015).
[9] K. V. Kravchyk, R. Widmer, R. Erni, R. J. C. Dubey, F. Krumeich, M. V. Kovalenko, and M. I. Bodnarchuk, Sci. Rep. **9**, 7988 (2019).
[10] X. Chen, H. Li, Y. Wu, H. Wu, L. Wu, P. Tan, J. Pan, and X. Xiong, J. Colloid Interface Sci. **476**, 132–143 (2016).
[11] J. Bai and X. Jiang, Anal. Chem. **85**, 8095–8101 (2013).
[12] K. Ding, J. Zeng, L. Jing, R. Qiao, C. Liu, M. Jiao, Z. Li, and M. Gao, Nanoscale **7**, 11075–11081 (2015).
[13] S. Goel, F. Chen, and W. Cai, Small **10**, 631–645 (2014).
[14] T. Sakamoto, H. Sunamura, H. Kawaura, T. Hasegawa, T. Nakayama, and M. Aono, Appl. Phys. Lett. **82**, 3032–3034 (2003).
[15] J. Tang, Z. Huo, S. Brittman, H. Gao, and P. Yang, Nat. Nanotechnol. **6**, 568–572 (2011).
[16] D. J. Chakrabarti and D. E. Laughlin, Bull. Alloy Phase Diagrams **4**, 254 (1983).
[17] I. Grozdanov and M. Najdoski, J. Solid State Chem. **114**, 469–475 (1995).
[18] I. Carbone, Q. Zhou, B. Vollbrecht, L. Yang, S. Medling, A. Bezryadina, F. Bridges, and G. B. Alers, J. Vac. Sci. Technol. A **29**, 051505 (2011).

[19]R. Nomura, K. Miyawaki, T. Toyosaki, and H. Matsuda, Chem. Vap. Deposition **2**, 174–179 (1996).
[20]A. L. Abdelhady, K. Ramasamy, M. A. Malik, P. O'Brien, S. J. Haigh, and J. Raftery, J. Mater. Chem. **21**, 17888–17895 (2011).
[21]Q. Lu, F. Gao, and D. Zhao, Nano Lett. **2**, 725–728 (2002).
[22]X. Chen, Z. Wang, X. Wang, R. Zhang, X. Liu, W. Lin, and Y. Qian, J. Cryst. Growth **263**, 570–574 (2004).
[23]Y. Zhao, H. Pan, Y. Lou, X. Qiu, J. Zhu, and C. Burda, J. Am. Chem. Soc. **131**, 4253–4261 (2009).
[24]U. Shamraiz, R. A. Hussain, and A. Badshah, J. Solid State Chem. **238**, 25–40 (2016).
[25]X.-H. Liao, N.-Y. Chen, S. Xu, S.-B. Yang, and J.-J. Zhu, J. Cryst. Growth **252**, 593–598 (2003).
[26]Y. Lu, X. Meng, G. Yi, and J. Jia, J. Colloid Interface Sci. **356**, 726–733 (2011).
[27]M. T. S. Nair and P. K. Nair, Semicond. Sci. Technol. **4**, 191–199 (1989).
[28]P. Vas-Umnuay and C.-h. Chang, ECS J. Solid State Sci. Technol. **2**, P120–P129 (2013).
[29]S. Lindroos, A. Arnold, and M. Leskelä, Appl. Surf. Sci. **158**, 75–80 (2000).
[30]C. D. Lokhande, Mater. Chem. Phys. **28**, 145–149 (1991).
[31]C. G. Munce, G. K. Parker, S. A. Holt, and G. A. Hope, Colloids Surf., A **295**, 152–158 (2007).
[32]E. Fatas, T. Garcia, C. Montemayor, A. Medina, E. G. Camarero, and F. Arjona, Mater. Chem. Phys. **12**, 121–128 (1985).
[33]A. M. Fernandez, P. J. Sebastian, J. Campos, O. Gomez-Daza, P. K. Nair, and M. T. S. Nair, Thin Solid Films **237**, 141–147 (1994).
[34]I. Grozdanov, C. K. Barlingay, and S. K. Dey, Mater. Lett. **23**, 181–185 (1995).
[35]L. Huang, R. A. Zingaro, E. A. Meyers, P. K. Nair, and M. T. S. Nair, Phosphorus, Sulfur Silicon Relat. Elem. **105**, 175–185 (1995).
[36]M. T. S. Nair, L. Guerrero, and P. K. Nair, Semicond. Sci. Technol. **13**, 1164 (1998).
[37]P. K. Nair, M. T. S. Nair, H. M. K. K. Pathirana, R. A. Zingaro, and E. A. Meyers, J. Electrochem. Soc. **140**, 754–759 (1993).
[38]A. A. Sagade and R. Sharma, Sens. Actuators, B **133**, 135–143 (2008).
[39]G. Hodes, *Chemical Solution Deposition of Semiconductor Films* (Marcel Dekker, New York, 2003).
[40]M. Chen, J. Zhao, and X. Zhao, Electrochim. Acta **56**, 5016–5021 (2011).
[41]J. K. Hedlund, T. G. Estrada, and A. V. Walker, Langmuir **36**, 3119–3126 (2020).
[42]C. G. Munce, G. K. Parker, and G. A. Hope, ECS Trans. **2**, 401–412 (2006).
[43]M. Xin, K. Li, and H. Wang, Appl. Surf. Sci. **256**, 1436–1442 (2009).
[44]C. Justin Raj, B. C. Kim, W.-J. Cho, W.-G. Lee, Y. Seo, and K.-H. Yu, J. Alloys Compd. **586**, 191–196 (2014).
[45]E. Güneri and A. Kariper, J. Alloys Compd. **516**, 20–26 (2012).
[46]N. K. Allouche, T. Ben Nasr, C. Guasch, and N. Kamoun Turki, C. R. Chim. **13**, 1364–1369 (2010).
[47]S. D. Sartale and C. D. Lokhande, Mater. Chem. Phys. **65**, 63–67 (2000).
[48]A. Ulman, Chem. Rev. **96**, 1533–1554 (1996).
[49]H. T. Evans, Am. Mineral. **66**, 807–818 (1981).
[50]J. C. W. Folmer and F. Jellinek, J. Less-Common Met. **76**, 153–162 (1980).
[51]A. Hooper, G. L. Fisher, K. Konstadinidis, D. Jung, H. Nguyen, R. Opila, R. W. Collins, N. Winograd, and D. L. Allara, J. Am. Chem. Soc. **121**, 8052–8064 (1999).
[52]G. L. Fisher, A. E. Hooper, R. L. Opila, D. L. Allara, and N. Winograd, J. Phys. Chem. B **104**, 3267–3273 (2000).
[53]G. L. Fisher, A. V. Walker, A. E. Hooper, T. B. Tighe, K. B. Bahnck, H. T. Skriba, M. D. Reinard, B. C. Haynie, R. L. Opila, N. Winograd, and D. L. Allara, J. Am. Chem. Soc. **124**, 5528–5541 (2002).
[54]J. K. Hedlund, A. A. Ellsworth, and A. V. Walker, ECS Trans. **86**, 89–101 (2018).
[55]M. L. Pacholski and N. Winograd, Chem. Rev. **99**, 2977–3006 (1999).
[56]D. L. Perry and J. A. Taylor, J. Mater. Sci. Lett. **5**, 384–386 (1986).
[57]M. C. Biesinger, Surf. Interface Anal. **49**, 1325–1334 (2017).
[58]I. Nakai, Y. Sugitani, K. Nagashima, and Y. Niwa, J. Inorg. Nucl. Chem. **40**, 789–791 (1978).
[59]M. Kundu, T. Hasegawa, K. Terabe, K. Yamamoto, and M. Aono, Sci. Technol. Adv. Mater. **9**, 035011 (2008).
[60]S. K. Chawla, N. Sankarraman, and J. H. Payer, J. Electron Spectrosc. Relat. Phenom. **61**, 1–18 (1992).
[61]NIST X-ray Photoelectron Spectroscopy Database, NIST Standard Reference Database Number 20, National Institute of Standards and Technology, Gaithersburg MD, 2000; retrieved 30 January, 2021.
[62]R. A. D. Pattrick, J. F. W. Mosselmans, J. M. Charnock, K. E. R. England, G. R. Helz, C. D. Garner, and D. J. Vaughan, Geochim. Cosmochim. Acta **61**, 2023–2036 (1997).
[63]J. K. Hedlund and A. V. Walker, Langmuir **36**, 682–688 (2020).
[64]Z. Jiang, W. Zhang, L. Jin, X. Yang, F. Xu, J. Zhu, and W. Huang, J. Phys. Chem. C **111**, 12434–12439 (2007).
[65]M. Ishii, K. Shibata, and H. Nozaki, J. Solid State Chem. **105**, 504–511 (1993).
[66]A. Adamou, A. Nicolaides, and C. Varotsis, Miner. Eng. **132**, 39–47 (2019).
[67]T. Safrani, J. Jopp, and Y. Golan, RSC Adv. **3**, 23066–23074 (2013).
[68]B. Minceva-Sukarova, M. Najdoski, I. Grozdanov, and C. J. Chunnilall, J. Mol. Struct. **410-411**, 267–270 (1997).
[69]W. H. R. Shaw and D. G. Walker, J. Am. Chem. Soc. **78**, 5769–5772 (1956).
[70]C. J. Doona and D. M. Stanbury, Inorg. Chem. **35**, 3210–3216 (1996).
[71]R. R. Das, T. R. Bhat, and J. Shankar, Indian J. Chem. **7**, 240–242 (1969).
[72]H. M. Ratajczak and L. Pajdowski, J. Inorg. Nucl. Chem. **36**, 459–461 (1974).
[73]A. Sarma, A.-C. Dippel, O. Gutowski, M. Etter, M. Lippmann, O. Seeck, G. Manna, M. K. Sanyal, T. F. Keller, S. Kulkarni, P. Guha, P. V. Satyam, and M. V. Zimmermann, RSC Adv. **9**, 31900–31910 (2019).
[74]W. Liang and M.-H. Whangbo, Solid State Commun. **85**, 405–408 (1993).
[75]D. Rickard and G. W. Luther, Chem. Rev. **107**, 514–562 (2007).
[76]D. Rickard, in *Developments in Sedimentology*, edited by D. Rickard (Elsevier, 2012), Vol. 65, pp. 31–83.
[77]M. Basafa and K. Hawboldt, J. Pet. Explor. Prod. Technol. **10**, 1603–1612 (2020).
[78]R. Steudel, in *Elemental Sulfur and Sulfur-Rich Compounds II*, Topics in Current Chemistry Vol. 231, edited by R. Steudel (Springer, Berlin, Heidelberg, 2003), pp. 127–152.
[79]R. A. Munson, Inorg. Chem. **5**, 1296–1297 (1966).
[80]D. Rosenthal and T. I. Taylor, J. Am. Chem. Soc. **82**, 4169–4174 (1960).
[81]E. Swift and F. Anson, Talanta **3**, 296–297 (1960).
[82]N. Isenberg, H. J. Kreger, and R. H. Middleton, J. Chem. Educ. **43**, 422 (1966).
[83]D. Rosenthal and T. I. Taylor, J. Am. Chem. Soc. **79**, 2684–2690 (1957).
[84]J. G. Speight, *Lange's Handbook of Chemistry*, 17th ed. (McGraw-Hill Education, New York, 2017).
[85]V. Chechik, R. M. Crooks, and C. J. M. Stirling, Adv. Mater. **12**, 1161–1171 (2000).
[86]A. E. Martell and R. M. Smith, *Critical Stability Constants* (Plenum Press, New York, 1974), Vol. 3, pp. 1–12.